Hydrogen Atom Adducts to the Amide Bond. Generation and Energetics of Amide Radicals in the Gas Phase

Erik A. Syrstad, Daniel D. Stephens, and František Tureček*

Department of Chemistry, Bagley Hall, Box 351700, University of Washington, Seattle, Washington 98195-1700

Received: June 12, 2002

The 1-hydroxy-1-(*N*-methyl)aminoethyl radical (**1**) represents a simple model system for hydrogen atom adducts to the amide bond in gas-phase peptide and protein ions relevant to electron capture dissociation (ECD). Radical **1** was generated in the rarefied gas phase by femtosecond electron transfer to the stable cation prepared by selective O-protonation of *N*-methylacetamide. The main dissociations of **1** were loss of the hydroxyl hydrogen atom and the *N*-methyl group in a 1.7:1 ratio, as deduced from product analysis and deuterium labeling. The dissociations that occur on the 4.1 microsecond time scale are driven by large Franck−Condon effects on collisional electron transfer that deposit 93−103 kJ mol^{-1} in the nascent radicals. Detailed analysis of the potential energy surface for dissociations of **1** revealed several conformers and isomeric transition states for dissociations of the O−H and N−CH_3 bonds. The experimental branching ratio is in quantitative agreement with RRKM calculations within the accuracy of the G2 potential energy surface and favors cleavage of the O—H bond in **1** and loss of H. This finding contrasts previously reported results, as discussed in the paper.

Introduction

Reactions of amino acids, peptides, and proteins with radicals generated in solution typically involve H atom abstraction followed by fragmentations, rearrangements, dimerization, and disproportionation of the transient reactive intermediates.[1] These chemical processes are of importance to areas ranging from medicine (aging, radiation damage, and oxidative stress)[2] to nuclear waste storage.[3] Analogous unimolecular dissociations have been observed for gas-phase peptide radical cations that undergo backbone cleavages and side-chain fragmentations upon collisional activation.[4] A different and unique type of reactivity has been reported for multiply protonated gas-phase peptide and protein cations that were partially reduced by capturing a thermal electron. This process, called electron capture dissociation (ECD),[5] results inter alia in backbone cleavage of the peptide ion that is of potential use for determining the amino acid sequence. A mechanism has been suggested (Scheme 1) consisting of electron capture by a charged group in the peptide cation, e.g., the ϵ-ammonium group of a protonated lysine residue or the protonated guanidine group of an arginine residue, to form a transient radical. This primary intermediate is expected to dissociate rapidly and exothermically by loss of a hydrogen atom that is captured by an adjacent amide bond to form an isomeric $C_{\alpha'}-C^{\bullet}(OH)-NH-C_{\alpha}$ radical. A radical-induced $N-C_{\alpha}$ bond cleavage in the latter results in fragmentation that yields structurally significant products belonging to the ***c*** and ***z*** series of sequence ions[6] (Scheme 1).

Although Scheme 1 provides a plausible explanation of some of the dissociations observed in ECD, the nature of the amide radical intermediates, their dissociation energetics, and kinetics are virtually impossible to investigate with large peptide or protein ions because of the multitude of ion structures involved and the ensuing multitude of dissociation pathways. In addition, ECD studies of peptide ions sometimes fail to account for complementary dissociation fragments of the ***c*** and ***z*** ion series, so that the postulated mechanisms cannot be verified by product analysis. Thus, it is advantageous to study simpler models that are amenable to high-level ab initio calculations to provide dissociation and transition state energies and that can be studied by experimental methods that allow complete analysis of radical dissociation products. In their early ECD study,[5b] Zubarev et al. reported density functional theory calculations of dissociations of a hydrogen atom adduct to *N*-methylacetamide (**1**) which was used as a model system. They concluded that although dissociation of the O−H bond in **1** should predominate at low excitation energies, at higher vibrational excitations the radical

SCHEME 1

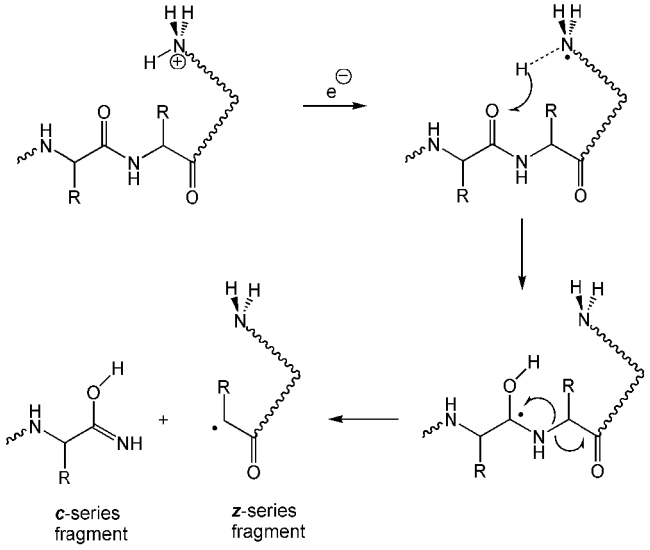

* To whom correspondence should be addressed. Phone: (206) 685-2041. Fax: (206) 685-3478. E-mail turecek@chem.washington.edu.

10.1021/jp021402r CCC: $25.00
Published on Web 12/04/2002

SCHEME 2

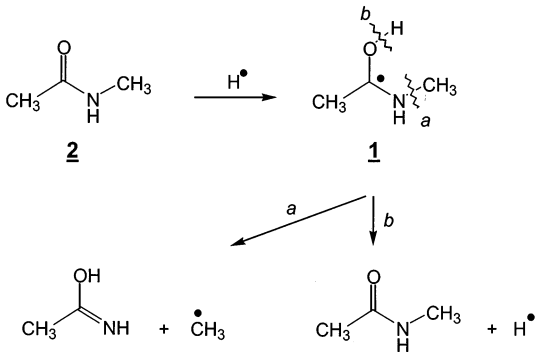

dissociation should be dominated by N−CH_3 bond cleavage analogous to dissociation leading to ***c*** and ***z*** ion series in larger peptide ions (Scheme 2).[6]

We now report a combined experimental and computational study of **1**, several of its isomers, and dissociation products. Radical **1** and its deuterium-labeled analogues **1a**−**1e** are generated specifically by femtosecond electron transfer in the gas phase, and their unimolecular dissociations are investigated by neutralization−reionization mass spectrometry[7] that provides detailed product analysis. We also report dissociation and transition state energies, obtained at high levels of ab initio theory, that are further used for Rice−Ramsperger−Kassel−Marcus (RRKM) calculations of unimolecular dissociation rate constants. We wish to point out that, despite its structural simplicity, **1** represents an intrinsically interesting system that shows a complex potential energy surface for unimolecular dissociations. In particular, we wish to compare the results of our high-level study with those of Zubarev et al.[5b] regarding radical **1** reactivity.

Experimental Section

Materials. *N*-methylacetamide (**2**) (Aldrich), acetone (Fisher, 99.8%), dimethyl disulfide (DMDS, Aldrich), ammonia (Scott Specialty Gases), and oxygen (Air Products) were used as received. Deuterium-labeled reagents D_2O and acetone-d_6 (both Cambridge Isotope Laboratories, 99.9% D) were also used as received.

***N*-Methylacetamide-N-*d* (2a).** *N*-methylacetamide (1.27 mL, 16.7 mmol) was stirred in 37.0 mL of D_2O at room temperature for 61 h, and the solvent was evaporated in vacuo.

***N*-Methylacetamide-2,2,2-d_3 (2b).** Neat $(CD_3CO)_2O$ (5 g, 0.046 mol, Aldrich, 99% D) was added dropwise under stirring to a 40% aqueous solution of methylamine (25 mL, 0.322 mol) that was cooled to 0 °C. After addition, the solution was allowed to warm to room temperature and stirred for 2 h. The solution was saturated with ammonium sulfate and the product was extracted in chloroform (5 × 20 mL). The chloroform extract was dried over anhydrous $MgSO_4$, the solvent was distilled off through a 20 cm Vigreux column, and $CD_3CONHCH_3$ was distilled, bp 110−115 °C/15 Torr. Yield: 2.7 g, 77%.

***N*-(Methyl-d_3)acetamide (2c).** Methyl-d_3 ammonium hydrochloride (5 g, 67 mmol, Aldrich, 99% D) was added slowly at 0 °C to 35 mL of 4 M NaOH aqueous solution. After 10 min, 7 g (69 mmol) of neat acetic anhydride was added dropwise at 0 °C. After 1 h, the reaction mixture was worked up as above and distilled at 15 Torr to give 3.6 g (71%) of $CH_3CONHCD_3$.

Methods. Measurements were performed on a tandem quadrupole acceleration−deceleration mass spectrometer described previously.[8] Cation $\mathbf{1}^+$ was generated in a tight chemical ionization (CI) source via selective protonation at oxygen of **2** using ammonia and acetone as the CI reagent gas. Similarly, selective protonation or deuteronation of **2** and **2a** with acetone and acetone-d_6 yielded cations $\mathbf{1a}^+$−$\mathbf{1c}^+$. Cations $\mathbf{1d}^+$ and $\mathbf{1e}^+$ were generated via protonation of **2b** and **2c**, respectively, with ammonia. In all cases, CI reagent gas pressure was maintained between 0.5 and 2.6 × 10^{-4} Torr as read on an ionization gauge near the diffusion pump intake. Typical ionization conditions were as follows: electron energy, 87−110 eV; emission current, 1 mA; and temperature, 188−227 °C. Cation-radical $\mathbf{2}^{+\bullet}$ was generated in a standard electron ionization (EI) source. Typical ionization conditions were as follows: electron energy, 70 eV; emission current, 500 μA; and temperature, 175−265 °C. Stable precursor ions were passed through a quadrupole mass filter operated in the radio frequency-only mode, accelerated to a total kinetic energy of 8250 eV, and neutralized in the collision cell floated at −8170 V. Dimethyl disulfide (DMDS) was introduced into the differentially pumped collision cell at a pressure that resulted in 70% transmittance of the precursor ion beam. The ions and neutrals were allowed to drift to a four segment conduit,[9] where the ions were reflected by the first segment floated at +250 V. Neutralization-collisional activation-reionization (NCR) experiments were performed by introducing helium as a collision gas into the conduit, at a pressure resulting in 50% transmittance of the precursor ion beam. The neutral flight times in standard neutralization−reionization mass spectrometry (NRMS) measurements were 4.1 μs. The fast neutral species were reionized in the second collision cell with oxygen at a pressure that resulted in 70% transmittance of the precursor ion beam. The ions formed in the second collision cell were decelerated, energy filtered, and analyzed by a second quadrupole mass filter operated at unit mass resolution. The instrument was tuned daily to maximize the ion current of reionized $CS_2^{+\bullet}$. Typical spectra consisted of 35−65 accumulated repetitive scans.

Collisionally activated dissociation (CAD) and metastable ion (MI) spectra were measured on a JEOL HX-110 double-focusing mass spectrometer of forward geometry (the electrostatic sector E precedes the magnet B). Collisions with air were monitored in the first field-free region at pressures resulting in 70% and 50% transmittance of the ion beam at 10 keV. The spectra were obtained by scanning E and B simultaneously while maintaining a constant B/E ratio (B/E-linked scan).

Calculations. Standard ab initio and density functional theory calculations were performed using the Gaussian 98 suite of programs.[10] Geometries were initially optimized using Becke's hybrid functional (B3LYP)[11] and the 6-31+G(d,p) basis set and reoptimized at 6-311+G(2d,p). Spin-unrestricted calculations (UB3LYP) were used for open-shell systems. In the UB3LYP calculations, $\langle S^2 \rangle$ operator expectation values ranged from 0.753 to 0.757 and 0.753 to 0.770 for local minima and transition state structures, respectively, indicating negligible spin contamination. Optimized structures were characterized by harmonic frequency analysis as local minima (all frequencies real) or first-order saddle points (one imaginary frequency). Zero-point vibrational energies (ZPVE) were calculated from B3LYP/6-311+G(2d,p) frequencies, which were scaled by 0.963 (ref 12). The rigid-rotor harmonic oscillator approximation was used in all thermochemical calculations. Single-point energies were calculated at two levels of theory. Composite G2(MP2) energies[13] were determined for all structures and transition states from MP2/6-311+G(3df,2p) and quadratic configuration interaction calculations, QCISD(T)/6-311G(d,p).[14] MP4(SDTQ) energies were calculated using an expanding basis set (6-311G(d,p), 6-311+G(d,p), and 6-311G(2df,p)) and used to determine

SCHEME 3

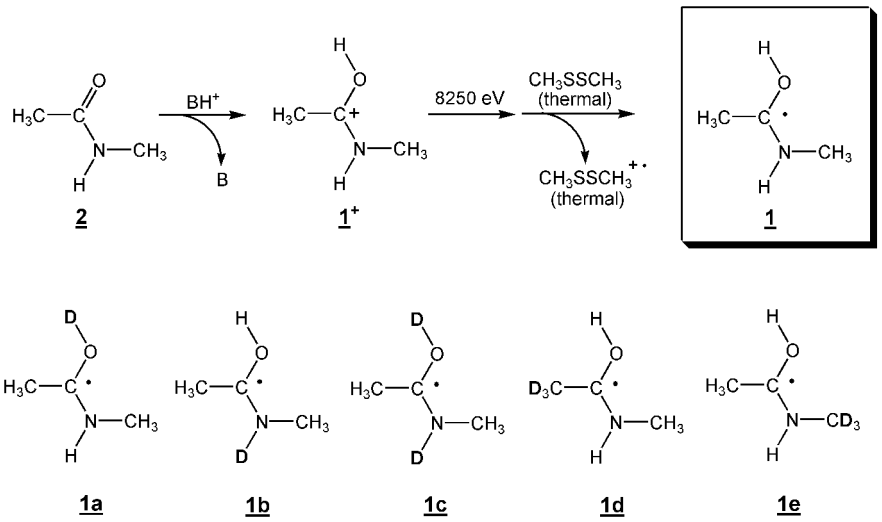

G2 energies[15] for several radicals, cations, and transition states of interest. Spin contamination in the UMP2, UMP4(SDTQ), and UQCISD(T) calculations was small for local minima, as shown by spin expectation values $\langle S^2 \rangle$ that ranged from 0.759 to 0.796. However, $\langle S^2 \rangle$ values ranged from 0.798 to 0.967 for transition states. Spin annihilation using Schlegel's projection method[16] (PMP2)[3] reduced the $\langle S^2 \rangle$ values to ≤ 0.76 for all structures.

Franck−Condon energies in vertical neutralization and reionization were taken as absolute differences between the total G2-(PMP2) energies of fully optimized ion or neutral structures and those in which an electron has been added to an optimized cation structure or subtracted from an optimized neutral structure. No zero-point corrections were applied to the calculated Franck−Condon energies.

RRKM calculations used Hase's program[17] that was recompiled for MS-DOS and run under Windows NT.[18] Vibrational state densities were obtained by direct count of quantum states in 2 kJ mol^{-1} steps for internal energies up to 205−310 kJ mol^{-1} above the threshold. The rotational states were treated adiabatically,[19] and the microscopic rate constants [$k(E,J,K)$] were Boltzmann-averaged over the thermal distribution of rotational J and K states pertaining to the ion source temperature.

Results and Discussion

Formation of 1−1e. Radicals **1**−**1e** were generated in two steps, as shown for **1** in Scheme 3. In the first step, *N*-methylacetamide (**2**) was selectively protonated at the oxygen atom with a gas-phase acid (BH^+) to yield cation $\mathbf{1}^+$. The protonation selectivity was ensured by the choice of the gas-phase acid and relied on the substantial difference in the topical proton affinities of the carbonyl oxygen (PA = 893 kJ mol^{-1}) and the nitrogen atom (PA = 833 kJ mol^{-1}) in **2** that were obtained by G2 calculations. Thus, only the more basic carbonyl oxygen can be protonated exothermically with a mild gas-phase acid such as NH_4^+ ($PA(NH_3)$ = 853 kJ mol^{-1}),[20,21] whereas endothermic protonation of the N-atom could not compete. In the next step, ion $\mathbf{1}^+$ was accelerated to 146 400 m s^{-1} corresponding to 8228 eV kinetic energy and discharged by collisional electron transfer from gaseous dimethyl disulfide. Because of the short duration of the electron-transfer collision, estimated at $<7 \times 10^{-15}$ s from the collision kinematics, radical **1** is formed by vertical electron transfer with the bond connectivity and geometry of the precursor cation.

The labeled cations and radicals were generated by combining selective protonation and deuteronation under H/D exchanging or nonexchanging conditions. Thus, cation $\mathbf{1a}^+$ was prepared from **2** by selective deuteronation with $(CD_3)_2COD^+$. This reagent ion was generated by self-deuteronation of acetone-d_6 which provides an essentially nonprototropic medium in the gas phase, such that the N-proton in **2** does not undergo exchange for D. Collisional reduction of $\mathbf{1a}^+$ with DMDS produced radical **1a**. Likewise, selective protonation of the carbonyl oxygen in the N−D labeled compound **2b** to form $\mathbf{1b}^+$ was achieved by reaction with $(CH_3)_2COH^+$,[22] followed by collisional reduction of the cation to produce radical **1b**. Radical **1c** was generated from amide **2b** by deuteronation with $(CD_3)_2COD^+$ forming $\mathbf{1c}^+$, followed by collisional reduction of the cation. Radicals **1d** and **1e** containing the label in nonexchangeable positions were generated by NH_4^+/NH_3 protonation of methyl-labeled *N*-methylacetamides **2d** and **2e**, respectively, followed by collisional electron transfer.

In addition to selective protonation with NH_4^+ and $(CH_3)_2COH^+$, we also used stronger gas-phase acids, $CH_3OH_2^+$ ($PA(CH_3OH)$ = 754 kJ mol^{-1}),[20,21] H_3O^+ ($PA(H_2O)$ = 691 kJ mol^{-1}),[20,21] and CH_5^+ ($PA(CH_4)$ = 544 kJ mol^{-1})[20,21] that should be able to protonate **2** at N and O nonselectively and produce mixtures of cation isomers. Collisional neutralization of cations produced by nonselective protonation was also studied, as discussed below.

Precursor Ion Structures and Dissociations. Because the structures of the incipient radicals **1**−**1e** are determined by those of the corresponding cations, we deemed it worthwhile to also investigate the properties of the precursor cations. Moreover, collisional reionization of neutral intermediates produces cations whose dissociations need to be deconvoluted from those of the radicals and molecules. Thus, some basic understanding of ion structures, energies, and dissociation mechanisms is necessary.

Four local minima were found for $\mathbf{1}^+$, viz *trans-anti*-$\mathbf{1}^+$, *cis-anti*-$\mathbf{1}^+$, *trans-syn*-$\mathbf{1}^+$, and *cis-syn*-$\mathbf{1}^+$ where cis and trans refer to the configuration of the amide group and syn and anti refer to the conformation of the OH group (Figure 1).[23] Of the ion isomers, *trans-anti*-$\mathbf{1}^+$ was the most stable conformer, followed by *cis-anti*-$\mathbf{1}^+$, *trans-syn*-$\mathbf{1}^+$, and *cis-syn*-$\mathbf{1}^+$ (Table 2). However, the small energy differences between *trans-anti*-$\mathbf{1}^+$ and *cis-anti*-$\mathbf{1}^+$ (ΔH_0 = 9 kJ mol^{-1}) and *trans-syn*-$\mathbf{1}^+$ (ΔH_0 = 10 kJ mol^{-1}) indicate that these two less stable conformers are also populated in the gas phase at 473−523 K, corresponding to the range of

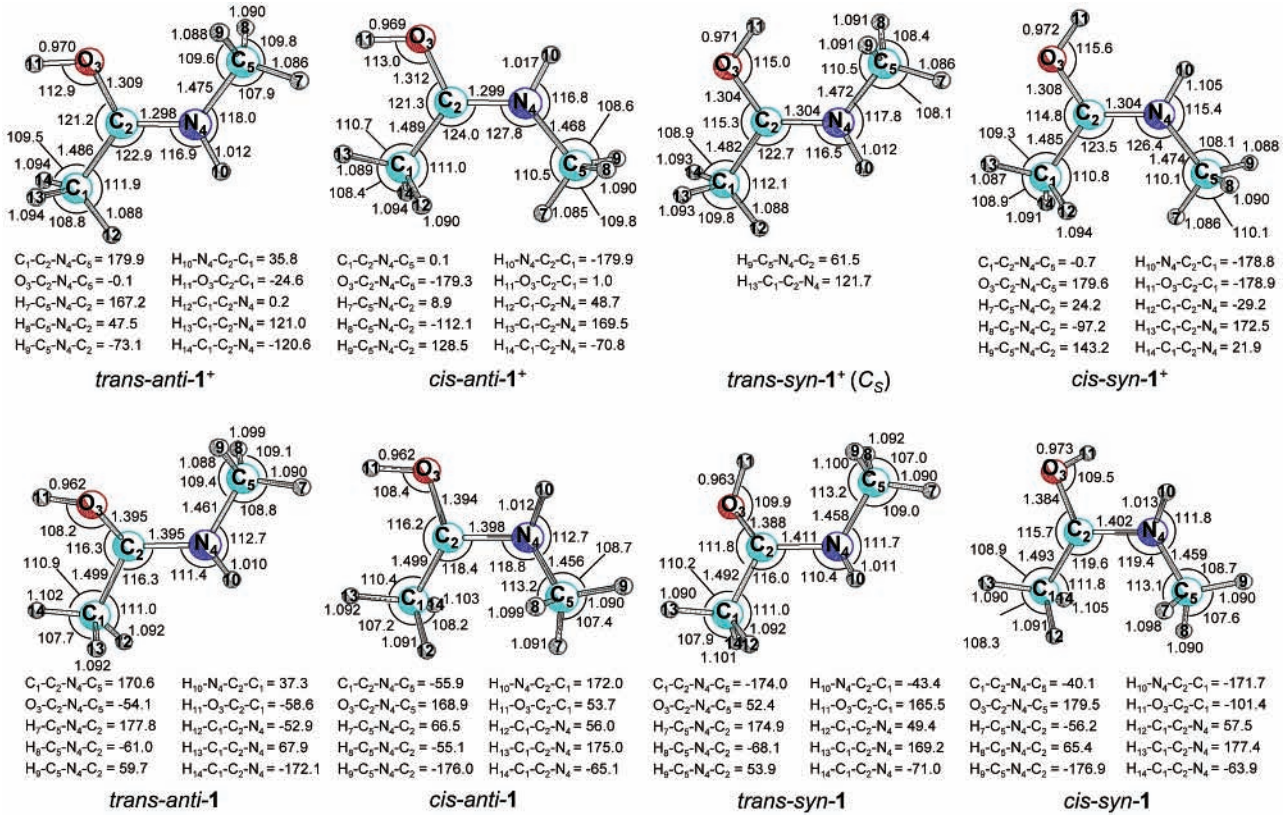

Figure 1. B3LYP/6-311+G(2d,p)-optimized structures of *trans-anti-*, *cis-anti-*, *trans-syn-*, and *cis-syn-***1** and -**1**$^+$. Bond lengths are in angstroms, and bond and dihedral angles are in degrees.

TABLE 1: Collisionally Activated Dissociation Spectra of Ions 1$^+$, 1a$^+$−1e$^+$ Relative Intensity[a]

m/z	**1**$^+$	**1a**$^+$	**1b**$^+$	**1c**$^+$	**1d**$^+$	**1e**$^+$	*m/z*	**1**$^+$	**1a**$^+$	**1b**$^+$	**1c**$^+$	**1d**$^+$	**1e**$^+$
76					4.3[b,3]	4.8[b,3]	40	1.2	1.6	1.6	1.3	0.9	1.9
75				23.7[b,1]	2.0	2.3	39	0.7	0.8	1.4			1.2
74		27.0[b,1]	6.1[b,1]	2.1[b,3]			38.5					1.5	1.7
73	5.9[b,3]	1.1	1.3				38	0.6	0.9	1.2	1.5	5.6	1.3
72	0.4	1.0	0.0				37.5		1.0	1.7	3.6		2.9
62					0.7	1.5	37	1.2	3.1	4.2		0.8	
61				1.6		2.8	36.5	5.7	0.8	1.4			
60		1.0	1.6	1.3		1.2	36	0.7					
59	1.2	1.4	2.9	1.7	3.2[b,4]	3.3[b,4]	35.5	0.5					
58	2.8	1.2	1.7		3.1	1.2	35						4.1[b,2]
57	0.7	2.6	1.2		0.9	1.1	34				3.6[b,4]	0.9	2.2
56	2.6[b,4]	0.8[b,4]	2.1[b,4]	2.7[b,6]	0.9	1.3	33		3.1[b,3]	4.8[b,3]	2.9[b,6]	5.1[b,2]	2.8
55	0.7	1.0	1.4	1.1			32	6.8[b,2]	3.0	3.6	4.4	3.8	5.9
54	1.1	0.7	1.5				31	4.3	4.3	7.1	3.6	5.3	2.0
53						1.1	30	9.4	4.1	2.5	2.1	4.0	2.6
52	0.6	0.8	1.3		0.7		29	1.5	2.0	4.4	3.9	2.7	4.3
51	0.5	0.7	-				28	5.5	4.9	2.9	2.3	4.9	2.6
50.5			1.2				27	1.5	1.4	2.2	1.5	1.1	1.4
48					1.2	1.4	26	0.8	1.2			0.7	1.3
47				1.2	1.2	1.3	25	0.5					
46		1.0	2.0	3.8	25.1[b,1]	1.0	19						1.5
45	1.4	2.7	3.8	2.4	4.9	1.5	18					1.8	2.0
44	5.4	3.4	2.7	2.7	6.5	5.7[b,5]	17					0.9	
43.5			1.3				16					0.8	
43	27.5[b,1]	14.4[b,2]	20.2[b,2]	18.7[b,2]	1.8	18.0[b,1]	15	1.8	1.8	2.5	1.7	1.1	2.0
42	4.2	3.2	4.3	3.1	1.1	4.3	14	0.7					
41	1.8	1.9	1.8	1.5	0.8	2.3							

[a] Relative to the sum of CAD ion intensities. [b] Dominant products of metastable ion dissociations, relative abundance 1 > 2 > ...

ion source temperatures used in our experiments, and can participate in ion dissociations. By comparison, cis−trans isomers of **2** differ by 10−12 kJ mol^{-1} in favor of the trans isomer.[24]

Metastable-ion (MI) and collisionally activated dissociations (CAD) of **1**$^+$ and its labeled isotopomers **1a**$^+$−**1e**$^+$ are summarized in Table 1. Elimination of methylamine is the dominant MI and CAD process yielding CH_3CO^+ at *m/z* 43 from **1**$^+$ and CD_3CO^+ at *m/z* 46 from **1d**$^+$. The other important dissociations are loss of H (*m/z* 73), CH_4 (*m/z* 58), H_2O (*m/z* 56), and ketene (*m/z* 32) and formation of $CH_2{=}NH_2^+$ (*m/z* 30). Deuterium labeling in **1c**$^+$ reveals that the loss of H involves mainly (92%) hydrogen atoms from the methyl groups (Table 1). Hence, the product cation-radicals correspond to a mixture of an *N*-

TABLE 2: Ion Relative Energies

species/reaction	relative energy[a] G2(MP2)[b]	relative energy[a] G2[b]	exp. (298 K)[c]
trans-anti-$\mathbf{1}^+$	0	0	
cis-anti-$\mathbf{1}^+$	9	9	
trans-syn-$\mathbf{1}^+$	11	10	
cis-syn-$\mathbf{1}^+$	20	20	
trans-anti-$\mathbf{1}^+$ (VI)[d]	137		
cis-anti-$\mathbf{1}^+$ (VI)[d]	140		
trans-syn-$\mathbf{1}^+$ (VI)[d]	127		
cis-syn-$\mathbf{1}^+$ (VI)[d]	141		
trans-anti-$\mathbf{1}^+ \rightarrow$ *trans*-**2** + H^+	887 (893)[e]	886 (893)[e]	889
cis-anti-$\mathbf{1}^+ \rightarrow$ *cis*-**2** + H^+	888 (893)[e]	887 (892)[e]	
trans-syn-$\mathbf{1}^+ \rightarrow$ *trans*-**2** + H^+	876 (883)[e]	876 (883)[e]	
cis-syn-$\mathbf{1}^+ \rightarrow$ *cis*-**2** + H^+	877 (883)[e]	876 (882)[e]	
$CH_3C{=}(O)NH_2CH_3^+ \rightarrow$ *trans*-**2** + H^+	827 (833)[e]	826 (832)[e]	
trans-anti-$\mathbf{1}^+ \rightarrow CH_3{-}N{=}C{-}CH_3^+ + H_2O$	113		
trans-anti-$\mathbf{1}^+ \rightarrow CH_3NH_3$- - $-CH_2{=}C{=}O^+$	115		
trans-anti-$\mathbf{1}^+ \rightarrow CH_2{=}C{=}O + CH_3NH_3^+$	155		160[f]
trans-anti-$\mathbf{1}^+ \rightarrow CH_3NH_2 + CH_3{-}C{=}O^+$	228		240[g]
trans-anti-$\mathbf{1}^+ \rightarrow HO{=}C{=}NH^+ + C_2H_6$	259		
trans-anti-$\mathbf{1}^+ \rightarrow CH_3C{=}(O)NH_2^{+\bullet} + CH_3^\bullet$	439		450
trans-anti-$\mathbf{1}^+ \rightarrow CH_3C(OH){=}NH^{+\bullet} + CH_3^\bullet$	485		
trans-anti-$\mathbf{1}^+ \rightarrow HO{=}C{=}NH^+ + 2\ CH_3^\bullet$	627		

[a] In units of kilojoules per mole at 0 K. [b] From spin-projected MP2 energies wherever it applies. [c] Experimental reaction enthalpies are based on thermochemical data from ref 21 unless stated otherwise. [d] Energy difference in kilojoules per mole between the vertically ionized cation and the optimized cation structure. [e] Topical proton affinities of **2** at 298 K. [f] Based on $\Delta H_{f,298}$ ($CH_2{=}C{=}O$) = −54 kJ mol^{-1}, see ref 31. [g] Based on $\Delta H_{f,298}$ ($CH_3C{=}O^+$) = 657 kJ mol^{-1}, see ref 32.

methylacetamide enol, $CH_2{=}C(OH){-}NHCH_3^{+\bullet}$, and the distonic ion, $CH_3C^+(OH){-}NH{-}CH_2^\bullet$. Elimination of methane selectively involves the acetyl methyl group, but the hydrogen atom is transferred nonselectively from the NH and OH groups. Elimination of water proceeds by specific transfer of the NH proton onto the hydroxyl group in $\mathbf{1}^+$.

The energetics of the dissociations observed in the MI and CAD spectra were obtained by G2(MP2) calculations as summarized in Table 2. Elimination of water is the lowest-energy dissociation which is 113 kJ mol^{-1} endothermic at the 0 K thermochemical threshold. Elimination of ketene forming $CH_3NH_3^+$ was the second most favorable dissociation that was calculated to require a threshold energy of $\Delta H_{rxn,0}$ = 155 kJ mol^{-1} (Table 2). Note that the elimination of ketene necessitates a rearrangement by transfer of two protons and may involve a hydrogen-bonded ion−molecule complex, $O{=}C{=}CH_2 \cdots H^+ \cdots H_2N{-}CH_3$, as an intermediate which is 115 kJ mol^{-1} higher in energy than *trans-anti*-$\mathbf{1}^+$ (Table 2). Elimination of methylamine was another low-energy dissociation of 228 kJ mol^{-1} threshold energy. In contrast, losses of methyl by dissociations of the C−C or N−C bonds are calculated to have >400 kJ mol^{-1} threshold energies (Table 2). It should be noted that the low-energy dissociations of $\mathbf{1}^+$ involve rearrangements by hydrogen transfer that are likely to have activation barriers that may exceed the threshold energies.

Radical Dissociations. The stability and dissociations of radicals **1**−**1e** were studied by NRMS. Collisional neutralization of $\mathbf{1}^+$ produced a small fraction of stable radicals (0.5% of the sum of NR ion intensities), which were detected following reionization as survivor ions at *m*/*z* 74 in the NR mass spectrum (Figure 2a). The primary unimolecular dissociations observed upon NR were loss of $H^\bullet$ (*m*/*z* 73) and loss of $CH_3^\bullet$ (*m*/*z* 59). Other dissociations proceeded in a consecutive fashion through the [C_3,N,O,H_7] and [C_2,H_4,N,O] molecules formed by the primary dissociations, as discussed below.

The loss of H from neutral **1** was distinguished from the analogous dissociation of reionized $\mathbf{1}^+$ by comparing the CAD and NR mass spectra of the isotopomers. NR of the OD-labeled

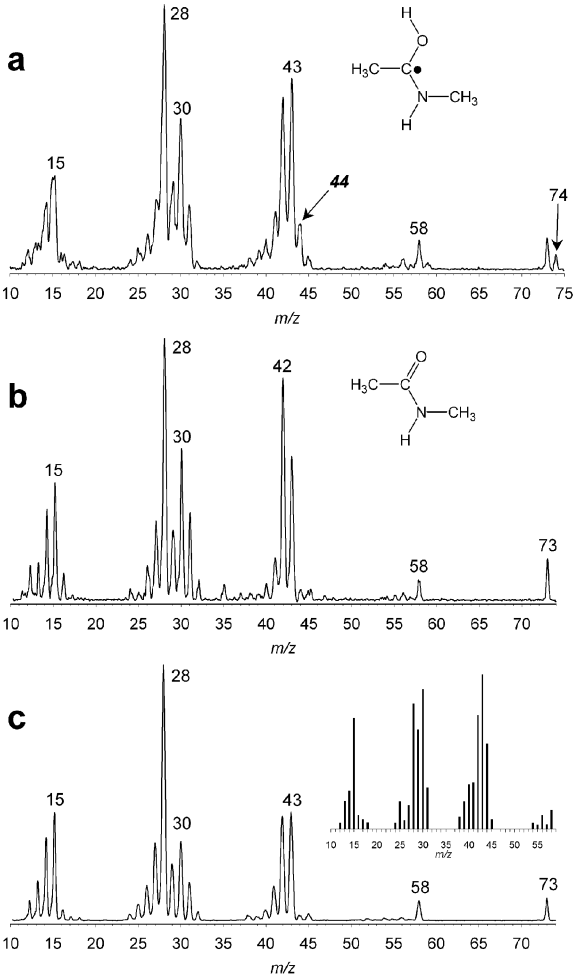

Figure 2. Neutralization (CH_3SSCH_3, 70% transmittance)−reionization (O_2, 70% transmittance) mass spectra of (a) $\mathbf{1}^+$ and (b) $\mathbf{2}^{+\bullet}$. (c) Neutralization (CH_3SSCH_3, 70% transmittance)-collisional activation (He, 50% transmittance)-reionization (O_2, 70% transmittance) mass spectrum of $\mathbf{2}^+$. Inset shows the difference spectrum from subtracting from (a) a weighed average of (b) and (c).

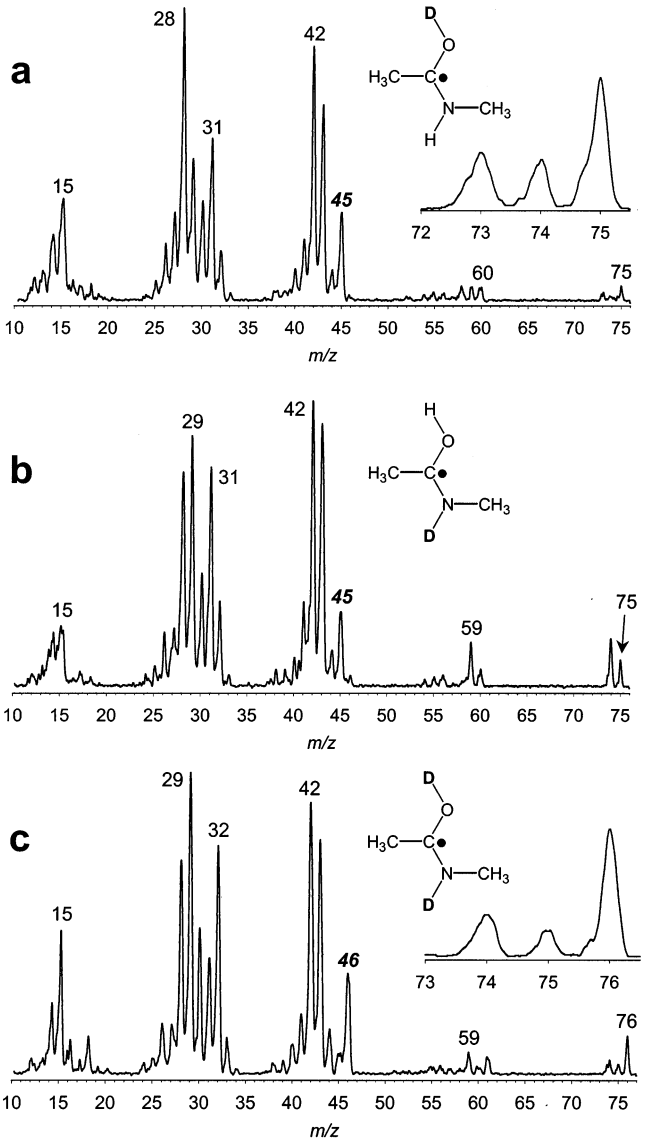

Figure 3. Neutralization (CH_3SSCH_3, 70% transmittance)−reionization (O_2, 70% transmittance) mass spectra of (a) $\mathbf{1a}^+$, (b) $\mathbf{1b}^+$, and (c) $\mathbf{1c}^+$.

ion $\mathbf{1a}^+$ showed 45% loss of H and 55% loss of D (Figure 3a, inset), whereas CAD of $\mathbf{1a}^+$ showed predominant (96%) loss of H (Table 1). Similarly, NRMS of N−CD_3 labeled $\mathbf{1e}^+$ showed no measurable loss of D (Figure 4b), whereas CAD of $\mathbf{1e}^+$ showed 33% loss of D and 67% loss of H. The combined evidence from all our labeling experiments pointed to loss of the H atom primarily from the OH group and to a lesser extent from the acetyl CH_3 group in dissociations of radical **1**. Hence, the main product of **1** dissociations is *N*-methylacetamide (**2**).

The origin of the other fragments in the NR mass spectrum of **1** was investigated in light of the formation of **2** as the primary dissociation product. To this end, we obtained the NR mass spectrum of $\mathbf{2}^{+\bullet}$ (Figure 2b) that contained most of the dissociation products also present in the NR spectrum of **1**. The similarity becomes even greater upon collisional activation of neutral **2**, followed by collisional reionization (NCR spectrum, Figure 2c), that yielded products in the *m*/*z* 15−73 mass region that had very similar relative intensities to those in the NR spectrum of **1** (Figure 2a). Because **2** is a stable molecule in the gas-phase, it is safe to conclude that the dissociations observed in its NR mass spectrum occur following collisional reionization and not in the stage of the neutral molecule. This conclusion is supported by the similarity of the NR and standard

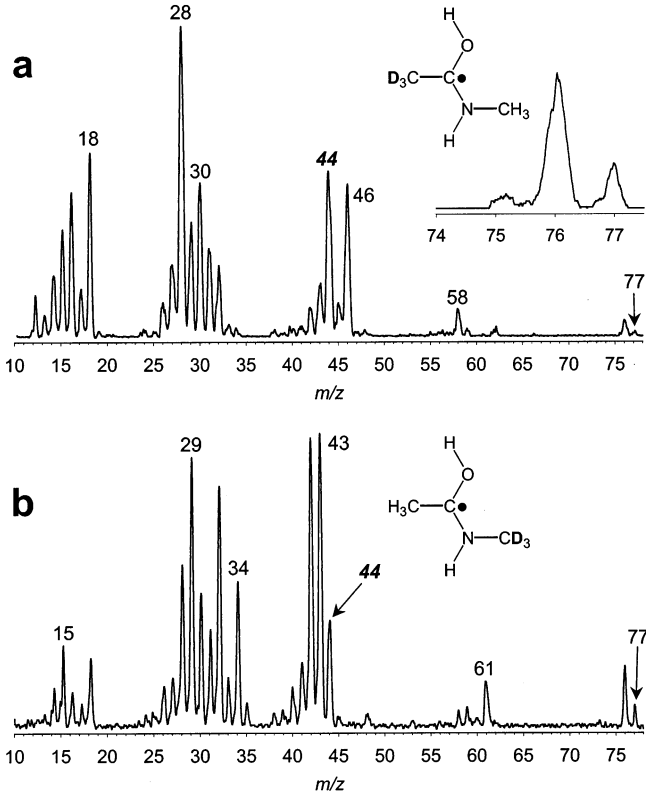

Figure 4. Neutralization (CH_3SSCH_3, 70% transmittance)−reionization (O_2, 70% transmittance) mass spectra of (a) $\mathbf{1d}^+$ and (b) $\mathbf{1e}^+$.

70-eV electron−ionization mass spectra that show identical major fragments at similar relative intensities.

A product in the NR spectrum of **1** that cannot be accounted for by consecutive **2** dissociations appears at *m*/*z* 44 (Figure 2a). Deuterium labeling shows unambiguously that this fragment is formed by loss of both methyl groups in **1** and corresponds to HO−C=NH^+. Comparison of the NR and CAD spectra of $\mathbf{1}^+$−$\mathbf{1e}^+$ further shows that the combined loss of two methyl groups is not due to contributions from dissociations of reionized $\mathbf{1}^+$−$\mathbf{1e}^+$. For example, the peak at *m*/*z* 44 shifts almost completely to *m*/*z* 45 in the NR spectra of $\mathbf{1a}^+$ and $\mathbf{1b}^+$, whereas in the corresponding CAD spectra there are substantial peaks remaining at *m*/*z* 44 (Table 1). An intermediate for the loss of the first methyl appears as a very weak peak at *m*/*z* 59 that shows the expected mass shift to *m*/*z* 60 in **1a** and **1b** because of the presence of OD and ND, respectively, and to *m*/*z* 61 in **1c**. Deuterium labeling of the methyl groups shows loss of the N−CH_3 methyl (*m*/*z* 62 in **1d**) but negligible loss of the acetyl methyl from **1e**, where the peak at *m*/*z* 62 is within the noise level. This points to an acetimino enol structure for the primary dissociation product at *m*/*z* 59, $CH_3C(OH)$=NH (**6**).

O−H/N−CH_3 Branching Ratio. To quantify the amounts of **2** and **6** formed by dissociation of **1**, we used the reference NR and NCR spectra of **2** that were weighted, mixed, and subtracted from the NR spectrum of **1** such as to annihilate the survivor peak of **2** at *m*/*z* 73. The difference spectrum (Figure 2c, inset) showed virtually no negative peaks and was assigned to represent reionized **6**. Note also that the difference spectrum shows no illogical losses that would be incompatible with structure **6**. The total NR ion currents in the weighted spectra of **2** and the difference spectrum for **6** were further scaled by the corresponding ratio of ionization cross sections $\sigma(\mathbf{6})/\sigma(\mathbf{2}) = 0.78$ that was estimated from the Fitch−Sauter additivity scheme.[25] This yielded a **2**/**6** branching ratio of 1.7.

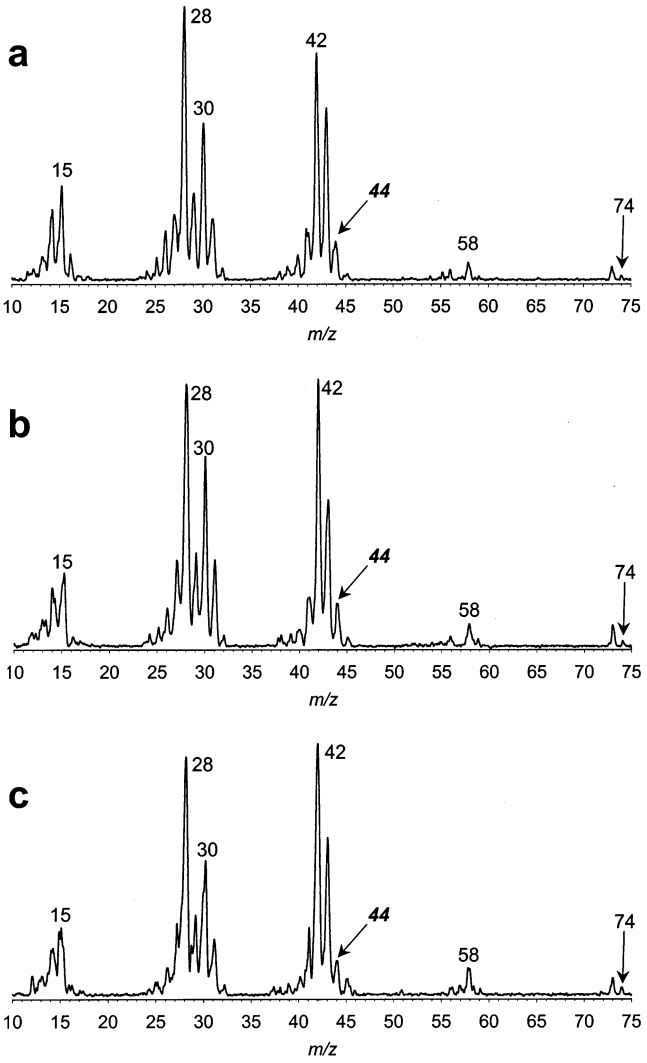

Figure 5. Neutralization (CH_3SSCH_3, 70% transmittance)−reionization (O_2, 70% transmittance) mass spectra of $\mathbf{1}^+$ following protonation with (a, top) $CH_3OH_2^+$, (b, middle) H_3O^+, and (c, bottom) CH_5^+.

Note that, because **6** is an unstable tautomer of acetamide, the corresponding cation−radical cannot be generated by direct ionization. Attempts were made to generate the reference ion $\mathbf{6}^{+\bullet}$ by alkene elimination from N-alkyl acetamide precursors, but dissociative ionization produced only low yields of $\mathbf{2}^{+\bullet}$.

Radicals from High-Energy Protonation of 2. Radicals formed by neutralization of cations produced by highly exothermic protonation with $CH_3OH_2^+$, H_3O^+, and CH_5^+ gave NR spectra that were similar to those shown in Figure 2. In particular, the spectra showed low-intensity survivor ions at *m*/*z* 74 and fragment ion relative intensities that pointed to dominant loss of the hydroxyl hydrogen and formation of **2** as a neutral intermediate (Figure 5). Interestingly, the ion relative intensities resembled those in the NR spectrum of $\mathbf{2}^{+\bullet}$ without collisional activation and indicated that the intermediate **2** was less excited. This may be due to a more efficient cooling of $\mathbf{1}^+$ in the ion source by collisions with CH_3OH, H_2O, and CH_4 than in the case of the acetone gas. The NR spectra in Figure 5 did not show an increased relative abundance of CH_3NH_2 (*m*/*z* 31) and its dissociation products that would indicate formation of the unstable $CH_3CO-NH_2^{\bullet}-CH_3$ radical by neutralization of N-protonated acetamide. $CH_3CO-NH_2^{\bullet}-CH_3$ was calculated to dissociate spontaneously to $CH_3CO^{\bullet}$ and methylamine.

In summarizing NR of **1**, loss of H from the OH group and loss of the *N*-methyl are the principal dissociations of radical **1** that occur in a 1.7:1 ratio.

Radical Structures and Energetics. Four local energy minima for radical **1** conformers were initially found by high-level ab initio calculations (Figure 1), e.g., *trans-anti*-**1**, *cis-anti*-**1**, *trans-syn*-**1**, and *cis-syn*-**1** that were analogous to the corresponding ion structures. The energy differences among the radical conformers were extremely small, as *cis-anti*-**1**, *trans-syn*-**1**, and *cis-syn*-**1** were only 1.9, 3.1, and 3.4 kJ mol^{-1} less stable than *trans-anti*-**1**, respectively. Interconversion of the radical isomers occurred through a combination of C_2-O_3 and C_2-N_4 bond rotations. The B3LYP/6-311+G(2d,p) potential energy surface (PES) was investigated for C_2-O_3 rotation in the most favored *trans-anti*-**1** radical, which had a dihedral angle $N_4-C_2-O_3-H_{11} = 166.1°$. Through C_2-O_3 rotation, two additional local minima were found. These rotamers had G2(MP2) energies of 1.5 and 3.2 kJ mol^{-1}, corresponding to dihedral angles $N_4-C_2-O_3-H_{11} = -26.3$ and +60.0, respectively. Energy barriers of 3.0, 2.8, and 3.7 kJ mol^{-1}, at dihedral angles $N_4-C_2-O_3-H_{11} = -127.1$, +25.0, and +98.2°, respectively, connected these radical rotamers to each other and to *trans-anti*-**1**. Interestingly, the PES for C_2-O_3 rotation did not include the *trans-syn*-**1** rotamer, as the pyramidal arrangement of C_1, O_3, and N_4 around C_2 was inverted between this radical and *trans-anti*-**1**, and this conformation was retained throughout the bond rotation.

Similar analysis of the PES for C_2-N_4 rotation from *trans-anti*-**1** found yet two more local minima, of dihedral angles $C_1-C_2-N_4-C_5 = -43.6$ and +55.9°, at 9.0 and 2.0 kJ mol^{-1} relative to *trans-anti*-**1**, respectively. Transition states connecting these rotamers, at dihedral angles $C_1-C_2-N_4-C_5 = -113.3$ and +88.7°, had relative energies of 17.8 and 23.5 kJ mol^{-1}, respectively. A true transition state (one imaginary frequency) was not found to connect the two above-mentioned local minima, because of a discontinuity in the B3LYP potential energy surface between a dihedral angle of 15 and 25°. However, this transition state was estimated to be, at most, 10−12 kJ mol^{-1} relative to *trans-anti*-**1**, so that rotamer interconversion would not be slowed at this energy barrier relative to the other two. Potential energy surfaces for C_2-O_3 and C_2-N_4 rotations starting from the other three known local minima were not determined, but it was clear that additional local minima likely existed. Franck−Condon energies were calculated by G2 for the vertical neutralization of $\mathbf{1}^+$ to **1** as 93 kJ mol^{-1} for *trans-anti*-$\mathbf{1}^+ \rightarrow$ *trans-anti*-**1**, 98 kJ mol^{-1} for *cis-anti*-$\mathbf{1}^+ \rightarrow$ *cis-anti*-**1**, 99 kJ mol^{-1} for *trans-syn*-$\mathbf{1}^+ \rightarrow$ *trans-syn*-**1**, and 103 kJ mol^{-1} for *cis-syn*-$\mathbf{1}^+ \rightarrow$ *cis-syn*-**1**. This pointed to substantial vibrational excitation in the ground electronic state (^2X) of **1** formed by vertical electron transfer.

Radical Dissociation Energetics. Transition state geometries for the loss of H from both O and N, as well as for loss of CH_3 from N, in **1** were determined at the UB3LYP/6-311+G(2d,p) level of theory (Figure 7). Potential energy surfaces along the dissociation coordinates were investigated for reaction pathways for O−H, N−H, and N−CH_3 cleavages by a PES-mapping method described previously.[26] Briefly, the appropriate bonds were stretched by 0.02 Å increments, whereas the remaining internal degrees of freedom were fully optimized, and each point near the transition state was treated with G2(MP2) single-point calculations, providing corrected PES profiles. Corrected saddle points were determined from polynomial fitting of these profiles and were used for G2 single-point energy calculations. These showed shortening of the transition state bond lengths from the

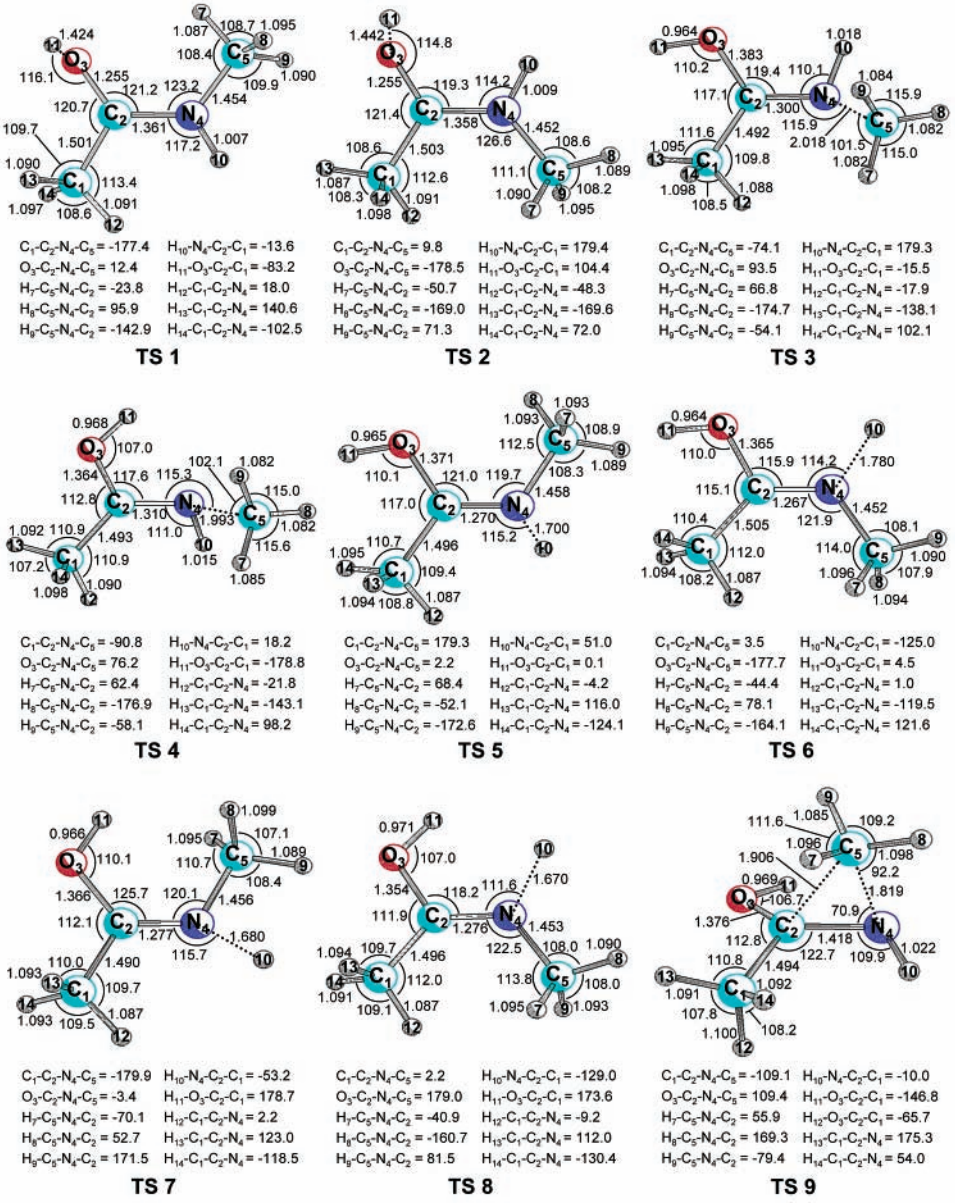

Figure 6. B3LYP/6-311+G(2d,p)-optimized structures of **TS1**−**TS9**.

UB3LYP-optimized saddle points, especially for N−H bond dissociation (Table 4). Dissociations of the O—H bonds encountered energy barriers that were identical for pairs of starting radicals having the same conformation of methyl groups around the amide bond. Starting from the *syn*- or *anti*- methyl conformations (**TS1** and **TS2**; 84 and 90 kJ mol^{-1}, respectively), these mirror-image, nearly planar saddle point geometries differed only in the orientation of the O−H bond being out of plane in either direction. Thus, *trans-anti*- and *trans-syn*-**1**, and *cis-anti*- and *cis-syn*-**1**, converged to *energetically*, but not *structurally*, identical transition states. Accordingly, the four (or more) starting isomers of **1** produced just two unique dissociation products (*cis*- and *trans*-**2** and H) from dissociation of O−H. However, N−H cleavage resulted in four distinct dissociation products, requiring a separate transition state connecting to each starting rotamer (**TS5**−**TS8**; 118, 132, 116, and 109 kJ mol^{-1}, respectively). In addition, transition states were found for N−CH_3 dissociation leading to the two (presumably) most favored products: *trans-syn*-**1** → **TS4** (84 kJ mol^{-1}), and *cis-anti*-**1** → **TS3** (93 kJ mol^{-1}). All pertinent relative energies are summarized in the potential energy diagram shown in Figure 7.

Five other [C_3,H_8,N,O] isomers were found to be local energy minima (Figure 8). The thermodynamically favored 2-hydroxypropane-2-aminyl isomers *syn*- and *anti*-**3** represented potential intermediates for methyl scrambling in radical **1**, but this process was associated with a substantial energy barrier of 214 kJ mol^{-1} (**TS9**, Figure 6). This indicated that methyl loss from **1** should proceed unambiguously, with no methyl scrambling. The 1-hydroxyethane-1-(*N*-methyl)aminyl isomers *syn*- and *anti*-**4** and the 1-(*N*-methyl)aminoethoxyl isomer **5** were found by G2 to be 7, 14, and 53 kJ mol^{-1} less stable than **1**, respectively (Table 3). As in the simpler amino(hydroxy)methyl system,[26] these radical stabilities follow the relative order of typical bond dissociation energies, BDE(O−H) > BDE(N−H) > BDE(C_{sp3}−H).[27]

The PES calculations pointed to the following conclusions. The conformers of **1** are nearly isoenergetic and can interconvert at internal energies that are way below the lowest dissociation threshold. Thus, any of the conformers can be available as a

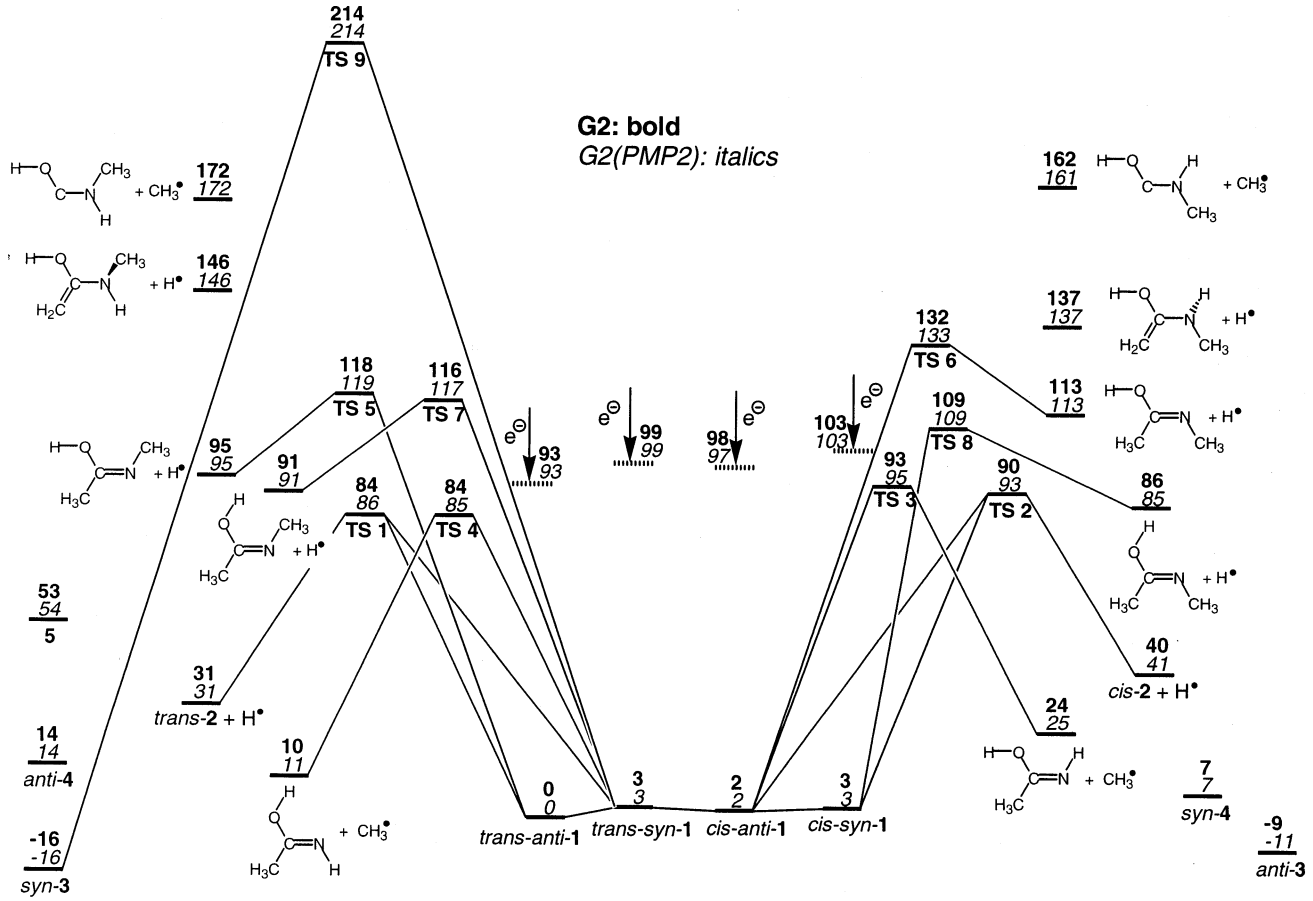

Figure 7. Potential energy diagram for dissociations of **1**.

reactant for a particular dissociation pathway. The transition states for loss of the O−H hydrogen atom and the N−CH_3 methyl group have very similar energies when starting from the same *syn*- or *anti*-O−H conformers. However, dissociations starting from the *trans*-amide conformers show slightly but significantly lower TS energies for loss of H and CH_3 than those starting from the cis conformers.

Dissociation Kinetics. To quantify the product formation by radical dissociations, we used the G2 energy barriers and UB3LYP/6-311+G(2d,p) harmonic frequencies and moments of inertia to calculate RRKM rate constants. The results of these calculations are shown in Figure 9. This figure provides a direct comparison of rate constants for competitive O−H, N−H, and N−CH_3 dissociations, with each calculated from the starting radical corresponding to the lowest energy barrier (see Figure 7). As discussed above, this comparison relied on the assumption that rotamer interconversion occurred much faster than any of the bond dissociations, producing an equilibrium mixture of starting radicals. The largest calculated barrier to isomerization was ∼24 kJ mol^{-1}, substantially lower than the most favored bond cleavage. The calculations indicated that, for the range of internal energies investigated (dissociation threshold to 390 kJ mol^{-1}), loss of H from **1** should occur predominately from the OH group. Unimolecular rate constants for O−H and N−H bond dissociations differed from each other by 2 orders of magnitude at about 150 kJ mol^{-1} internal energy and converged to 1 order of magnitude at 265 kJ mol^{-1}. However, O−H and N−CH_3 bond dissociations were predicted to be very competitive at all energies, as expected by their identical energy barriers. In contrast to the previous report of Zubarev et al.,[5b] our calculations indicate that the dissociation of the O−H bond becomes faster at very high excitations of the radical (Figure 10). This result is to be expected from RRKM theory for competitive dissociations through nearly isoenergetic but nonequivalent transition states. In this special case, the ratio of rate constants is given by eq 1

$$k(\mathrm{O\cdots H})/k(\mathrm{N\cdots CH_3}) \approx \mathrm{W^{\ddagger}(O\cdots H)/W^{\ddagger}(N\cdots CH_3)} \quad (1)$$

where $W^{\ddagger}(O\cdots H)$ and $W^{\ddagger}(N\cdots CH_3)$ are the quantum state counts in the transition states for the corresponding bond dissociations.[28] Hence, at sufficiently high internal energies where the nuances in quantum state combinations and small differences in the potential energy barriers become irrelevant, the different vibrational frequencies for the stretching modes, $\nu(O{-}H) > \nu(N{-}CH_3)$, cause that the transition state for the O···H bond cleavage that preserves the softer N−CH_3 stretching vibration can be realized in a greater number of quantum states and will allow faster dissociation, as shown in Figure 10.

Dissociation Mechanisms Relevant to NRMS of 1. The competitive dissociations of **1** by loss of H and CH_3 that are triggered by femtosecond electron transfer depend on the internal energy imparted in the radical. The internal energy of vertically formed **1** contains contributions from the internal energy of the precursor ion (E_{ion}), the Franck−Condon energy gained upon electron transfer (E_{FC}), and the excitation energy of the particular electronic state (ΔE_{exc}). We have shown previously[29] that the most probable internal energy $\langle E_{int}\rangle$ of radicals produced by NR in the ground electronic state ($\Delta E_{exc} = 0$) can be expressed as a simple sum of two terms, e.g., $\langle E_{int}\rangle = E_{ion} + E_{FC}$. Of these, E_{FC} in **1** was obtained by G2 calculations as 93 kJ mol^{-1}. E_{ion} was estimated as 95−99 kJ mol^{-1} from the thermal energy of **2** at the typical ion source temperature (30−34 kJ mol^{-1} at 460−500 K) and an ≈80% fraction of protonation exothermicity (65

TABLE 3: Radical Relative Energies

species/reaction	relative energy[a] G2(MP2)[b]	G2[b]
trans-anti-**1**	0	0
cis-anti-**1**	2	2
trans-syn-**1**	3	3
cis-syn-**1**	3	3
trans-anti-**1** (VN)[c]	93	93
cis-anti-**1** (VN)[c]	96	96
trans-syn-**1** (VN)[c]	96	96
cis-syn-**1** (VN)[c]	100	100
syn-**3**	−16	−16
anti-**3**	−11	−9
syn-**4**	7	7
anti-**4**	14	14
5	54	53
trans-anti-**1** → *trans*-**2** + H$^\bullet$	31	31
cis-anti-**1** → *cis*-**2** + H$^\bullet$	39	39
trans-syn-**1** → *trans*-**2** + H$^\bullet$	28	28
cis-syn-**1** → *cis*-**2** + H$^\bullet$	37	37
trans-anti-**1** → *trans-anti*-$CH_3C(OH)$═NCH_3 + H$^\bullet$	95	95
cis-anti-**1** → cis-*anti*-$CH_3C(OH)$═NCH_3 + H$^\bullet$	111	111
trans-syn-**1** → trans-*syn*-$CH_3C(OH)$═NCH_3 + H$^\bullet$	88	88
cis-syn-**1** → *cis-syn*-$CH_3C(OH)$═NCH_3 + H$^\bullet$	84	84
trans-anti-**1** → *trans-anti*-CH_2═$C(OH)NHCH_3$ + H$^\bullet$	146	146
cis-anti-**1** → *cis-anti*-CH_2═$C(OH)NHCH_3$ + H$^\bullet$	135	135
trans-anti-**1** → *trans-anti*-$CH_3C(OH)NHCH_2$ + H$^\bullet$	285	-
cis-anti-**1** → *cis-anti*-$CH_3C(OH)NHCH_2$ + H$^\bullet$	284	-
cis-anti-**1** → *anti*-$CH_3C(OH)$═NH + $CH_3^\bullet$	23	22
trans-syn-**1** → *syn*-$CH_3C(OH)$═NH + $CH_3^\bullet$	7	7
trans-anti-**1** → $C(OH)NHCH_3$ + $CH_3^\bullet$	172	172
cis-anti-**1** → $C(OH)NHCH_3$ + $CH_3^\bullet$	160	160
trans-anti-**1** → C(OH)═NH$^\bullet$ + 2 $CH_3^\bullet$	439	-
trans-anti-**1** → C(OH)═NH$^\bullet$ + C_2H_6	71	70
TS1	86	84
TS2	93	90
TS3	95	93
TS4	85	84
TS5	119	118
TS6	133	132
TS7	117	116
TS8	109	109
TS9	214	214

[a] In units of kilojoules per mole at 0 K. [b] From spin-projected MP2 energies wherever it applies. [c] Energy difference in kilojoules per mole between the vertically neutralized radical and the optimized radical structures.

TABLE 4: Transition State Bond Lengths

species	d(X−Y)[a,b] B3LYP[c]	G2(MP2)[d]
TS1	1.424	1.383
TS2	1.442	1.392
TS3	2.018	1.990
TS4	1.993	1.980
TS5	1.700	1.580
TS6	1.780	1.629
TS7	1.680	1.560
TS8	1.670	1.587

[a] In units of angstroms. [b] X = O, N; Y = H, CH_3. [c] UB3LYP/6-311+G(2d,p) saddle point. [d] G2(MP2) corrected saddle point; from spin-projected MP2 energies.

kJ mol^{-1}).[30] These energy contributions were calculated for *trans-anti*-**1**, as the precursor cation equilibrium should favor this isomer, similar to the preference that has been determined for protonated formamide cations.[26] From the energy terms for E_{ion} and E_{FC} one obtains $\langle E_{int}\rangle$ = 188−192 kJ mol^{-1} in *trans-anti*-**1**. This is sufficient to drive dissociation of the O−H, N−H, and N−CH_3 bonds, which all require lower energies in the corresponding transition states.

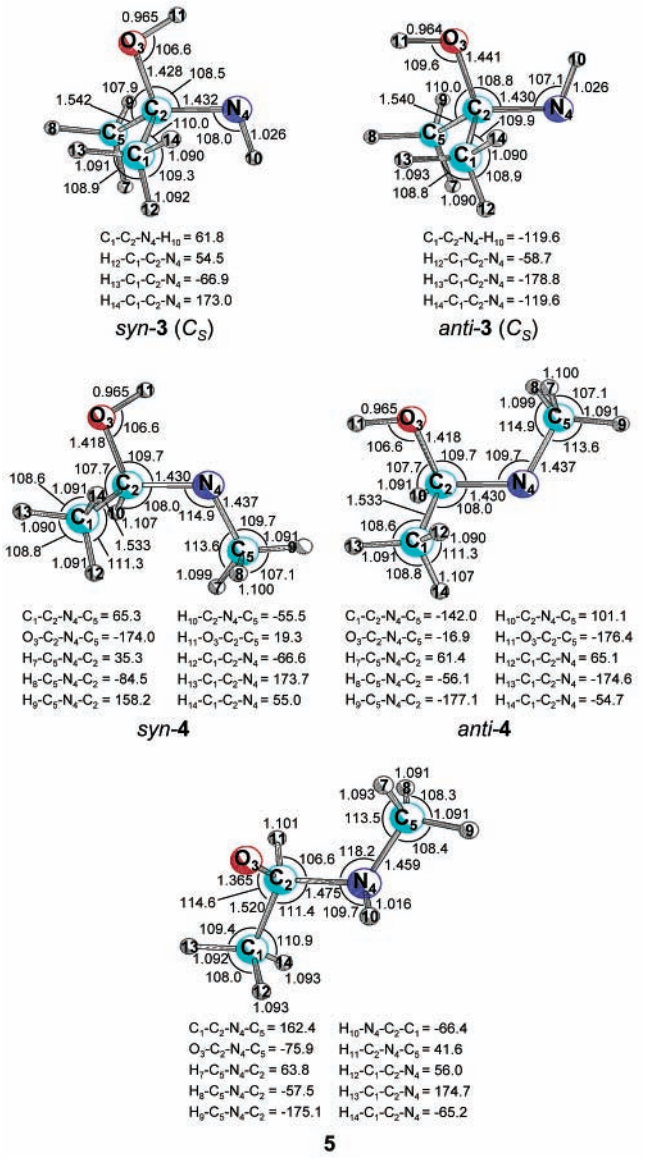

Figure 8. B3LYP/6-311+G(2d,p)-optimized structures of *syn*- and *anti*-**3**, -**4**, and **5**.

Regarding competitive dissociations of O−H and N−H bonds in **1**, RRKM rate constants obtained for $\langle E_{int}\rangle$ = 190 kJ mol^{-1} predict branching ratios to be k(O—H)/k(N—H) ≈ 25 (Figure 9), in qualitative agreement with experimental observations. In addition, branching ratios k(X−D)/k(X−H) (X = O and N) were determined experimentally and computationally for loss of (H,D) from the most favored starting isomer in O−D labeled **1a**$^+$ and N−D labeled **1b**$^+$. NR of **1a**$^+$ shows a branching ratio k(O−D)/k(N−H) = 1.21, compared to a value of 13.0 predicted from RRKM data (Figure 9). In **1b**$^+$, the NR spectrum indicates a branching ratio k(N−D)/k(O−H) = 0, compared to a value of 0.013 predicted by RRKM calculations. Clearly, however, the peaks for O−H and N−H dissociation products in the NR spectra contained possible contributions from ionic C−H bond cleavage. In addition, consecutive dissociations, mostly following reionization, likely depleted the [M−D] and [M−H] NR signals disproportionately, somewhat compromising quantitative comparisons.

Regarding competitive dissociations of the O−H and N−CH_3 bonds, RRKM calculations predict the energy-dependent branch-

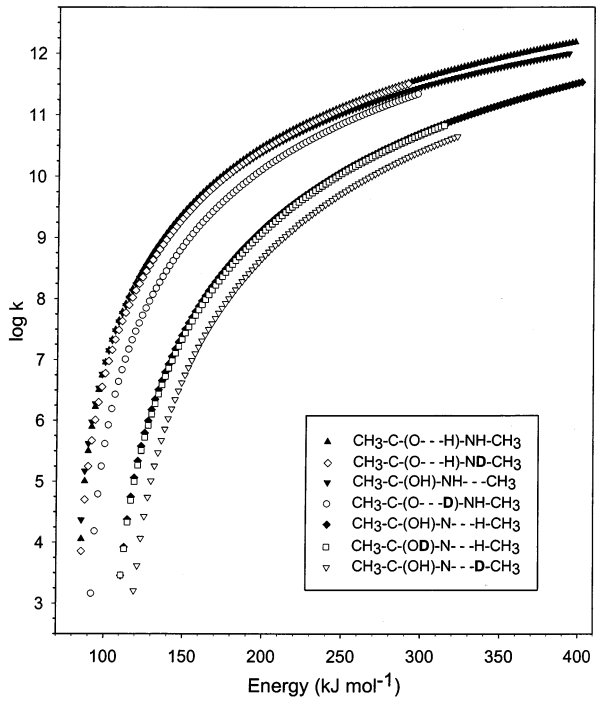

Figure 9. RRKM unimolecular rate constants (log, s^{-1}) for dissociations of **1**.

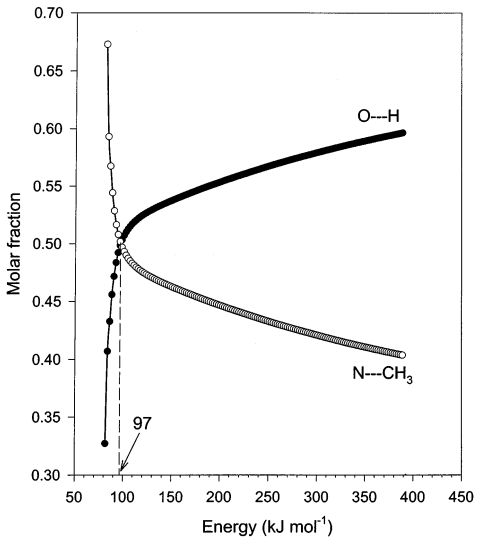

Figure 10. Energy dependence of the branching ratio for the dissociations of the O−H and N−CH_3 bonds in **1** forming **2** and **6**, respectively.

ing ratios that are depicted in Figure 10 for the G2-calculated TS energies. At near-threshold energies (84 kJ mol^{-1}), loss of CH_3 is about twice as fast as loss of H. However, the curves cross at E_{int} = 97 kJ mol^{-1} and the k(O−H)/k(N−CH_3) branching ratio increases to 1.2 at $\langle E_{int}\rangle$ = 190 kJ mol^{-1} and converges to 1.5 at $E_{int} \geq$ 400 kJ mol^{-1}. Full quantitative agreement with the branching ratio from NR dissociations can be achieved by using eq 2 where $P(E)$ is an energy distribution function, $E_{a,H}$ and $E_{a,CH3}$ are the pertinent TS energies, k_H and k_{CH3} are the RRKM unimolecular rate constants, and τ is the time

$$\frac{[\mathbf{2}]}{[\mathbf{6}]} = \frac{\int_0^\tau \mathrm{d}t \int_{E_{a,H}}^\infty k_H(E)P(E)\mathrm{e}^{-(k_H+k_{CH3})t}\,\mathrm{d}E}{\int_0^\tau \mathrm{d}t \int_{E_{a,CH3}}^\infty k_{CH3}(E)P(E)\mathrm{e}^{-(k_H+k_{CH3})t}\,\mathrm{d}E} \qquad (2)$$

for neutral dissociation (4.1 μs). $P(E)$ is given by eq 3,[29] where the parameters E_0 and W were set to 73 and 117 kJ mol^{-1} to give the mean internal energy $\langle E\rangle$ = 190 kJ mol^{-1} (vide supra)

$$P(E) = \frac{4(E - E_0)}{W^2} e^{-2(E - E_0)/W} \qquad (3)$$

while allowing for 0.5% relative abundance of undissociated **1** to reproduce the NR spectrum (cf. Figure 2a). The experimental ratio [**2**]/[**6**] = 1.7 is matched by lowering the G2 value for $E_{a,H}$ from 81.2 to 78.7 kJ mol^{-1}. Note that a 2.5 kJ mol^{-1} adjustment is well within the accuracy of G2 energy calculations (4 kJ mol^{-1}).[13,15] Hence, theory and experiment are in near perfect quantitative agreement.

Conclusions

The 1-hydroxy-1-(*N*-methyl)aminoethyl radical is both thermodynamically and kinetically stable in the gas phase. When formed by fast electron transfer to O-protonated acetamide, the radical acquires ca. 100 kJ mol^{-1} internal energy through Franck−Condon effects that drive dissociations of the O−H and N−CH_3 bonds. The experimental branching ratio of 1.7:1 that prefers the O−H bond dissociation is reproduced by RRKM calculations of the unimolecular rate constants within the accuracy of the G2 potential energy surface. This study shows that radicals derived from *N*-methylacetamide do not represent the best model for electron capture dissociation, where N−C bond dissociations leading to backbone fragmentation predominate. More sophisticated models that mimic the electronic properties of peptide radicals and dissociation products are needed for elucidating ECD mechanisms.

Acknowledgment. Support of this work by NSF (CHE-009-0930) is gratefully acknowledged. Support for the Computational Chemistry Facility was provided jointly by NSF-CRIF (CHE-9808182) and the University of Washington. We thank Dr. Martin Sadílek for assistance with CAD spectra measurements.

References and Notes

(1) Hawkins, C. L.; Davies, M. J. *Biochim. Biophys. Acta* **2001**, *1504*, 196−219.

(2) (a) Berlett, B.; Stadtman, E. R. *J. Biol. Chem.* **1997**, *272*, 20313−20316. (b) Schoneich, C. *Exp. Gerontol.* **1999**, *34*, 19−34.

(3) (a) Wisniowski, P.; Carmichael, I.; Fessenden, R. W.; Hug, G. L. *J. Phys. Chem. A* **2002**, *106*, 4573−4580. (b) Meisel, D. M.; Camaioni, D.; Orlando, T. M. In *ACS Symposium Series*; American Chemical Society: Washington, DC, 2001; Vol. 778, pp 342−361.

(4) (a) Gatlin, C. L.; Tureček, F.; Vaisar, T. *J. Am. Chem. Soc.* **1995**, *117*, 3637−3638. (b) Vaisar, T.; Gatlin, C. L.; Tureček, F. *J. Am. Chem. Soc.* **1996**, *118*, 5314−5315. (c) Chu, I. K.; Rodriquez, C. F.; Lau, T.-C.; Hopkinson, A. C.; Siu, K. W. M. *J. Phys. Chem. B* **2000**, *104*, 3393−3397. (d) Wee, S.; O'Hair, R. A. J.; McFadyen, W. D. *Rapid Commun. Mass Spectrom.* **2002**, *16*, 884−890.

(5) (a) Zubarev, R. A.; Kelleher, N. L.; McLafferty, F. W. *J. Am. Chem. Soc.* **1998**, *120*, 3265−3266. (b) Zubarev, R. A.; Kruger, N. A.; Fridriksson, E. K.; Lewis, M. A.; Horn, D. M.; Carpenter, B. K.; McLafferty, F. W. *J. Am. Chem. Soc.* **1999**, *121*, 2857−2862. (c) Cooper, H. J.; Hudgins, R. R.; Hakansson, K.; Marshall, A. G. *J. Am. Soc. Mass Spectrom.* **2002**, *13*, 241−249.

(6) For peptide fragment nomenclature see (a) Roepstorff, P.; Fohlman, J. *Biomed. Mass Spectrom.* **1984**, *11*, 601. (b) Biemann, K. *Biomed. Environm. Mass Spectrom.* **1988**, *16*, 99.

(7) For comprehensive reviews of the technique, see: (a) Wesdemiotis, C.; McLafferty, F. W. *Chem. Rev.* **1987**, *87*, 485−500. (b) Holmes, J. L. *Mass Spectrom. Rev.* **1989**, *8*, 513−539. (c) Schalley, C. A.; Hornung, G.; Schroder, D.; Schwarz, H. *Chem. Soc. Rev.* **1998**, *27*, 91−104. (d) Zagorevskii, D. V.; Holmes, J. L. *Mass Spectrom. Rev.* **1999**, *18*, 87−118.

(8) Tureček, F.; Gu, M.; Shaffer, S. A. *J. Am. Soc. Mass Spectrom.* **1992**, *3*, 493−501.

(9) Tureček, F. *Org. Mass Spectrom.* **1992**, *27*, 1087−1097.

(10) Frisch, M. J.; Trucks, G. W.; Schlegel, H. B.; Scuseria, G. E.; Robb, M. A.; Cheeseman, J. R.; Zakrzewski, V. G.; Montgomery, J. A., Jr.; Stratmann, R. E.; Burant, J. C.; Dapprich, S.; Millam, J. M.; Daniels, A.

D.; Kudin, K. N.; Strain, M. C.; Farkas, O.; Tomasi, J.; Barone, V.; Cossi, M.; Cammi, R.; Mennucci, B.; Pomelli, C.; Adamo, C.; Clifford, S.; Ochterski, J.; Petersson, G. A.; Ayala, P. Y.; Cui, Q.; Morokuma, K.; Malick, D. K.; Rabuck, A. D.; Raghavachari, K.; Foresman, J. B.; Cioslowski, J.; Ortiz, J. V.; Stefanov, B. B.; Liu, G.; Liashenko, A.; Piskorz, P.; Komaromi, I.; Gomperts, R.; Martin, R. L.; Fox, D. J.; Keith, T.; Al-Laham, M. A.; Peng, C. Y.; Nanayakkara, A.; Gonzalez, C.; Challacombe, M.; Gill, P. M. W.; Johnson, B. G.; Chen, W.; Wong, M. W.; Andres, J. L.; Head-Gordon, M.; Replogle, E. S.; Pople, J. A. *Gaussian 98*, revision A.6; Gaussian, Inc.: Pittsburgh, PA, 1998.

(11) (a) Becke, A. D. *J. Chem. Phys.* **1993**, *98*, 1372−1377. (b) Stephens, P. J.; Devlin, F. J.; Chabalowski, C. F.; Frisch, M. J. *J. Phys. Chem.* **1994**, *98*, 11623−11627.

(12) Rauhut, G.; Pulay, P. *J. Phys. Chem.* **1995**, *99*, 3093−3100.

(13) Curtiss, L. A.; Raghavachari, K.; Pople, J. A. *J. Chem. Phys.* **1993**, *98*, 1293−1298.

(14) Pople, J. A.; Head-Gordon, M.; Raghavachari, K. *J. Chem. Phys.* **1987**, *87*, 5968−5975.

(15) Curtiss, L. A.; Raghavachari, K.; Trucks, G. W.; Pople, J. A. *J. Chem. Phys.* **1991**, *94*, 7221−7230.

(16) (a) Schlegel, H. B. *J. Chem. Phys.* **1986**, *84*, 4530−4534. (b) Mayer, I. *Adv. Quantum Chem.* **1980**, *12*, 189−262.

(17) Zhu, L.; Hase, W. L. *Quantum Chemistry Program Exchange*; Indiana University: Bloomington, IN, 1994; Program No. QCPE 644.

(18) Frank, A. J.; Sadilek, M.; Ferrier, J. G.; Tureček, F. *J. Am. Chem. Soc.* **1997**, *119*, 12343−12353.

(19) Zhu, L.; Hase, W. L. *Chem. Phys. Lett.* **1990**, *175*, 117−124.

(20) Hunter, E. P.; Lias, S. G. *J. Phys. Chem. Ref. Data*, **1998**, *27*, 413−656.

(21) http://webbook.nist.gov/chemistry

(22) Although the proton affinity of acetone (812 kJ mol^{-1}) makes $(CH_3)_2COH^+$ sufficiently acidic to protonate the amide nitrogen in **2** of *PA* = 833 kJ mol^{-1}, this protonation cannot compete kinetically with that of the C═O group where the thermochemistry predicts it to occur at the collision rate limit. For the relationship between proton-transfer kinetics and thermochemistry, see Bouchoux, G.; Salpin, J. Y.; Leblanc, D. *Int. J. Mass Spectrom. Ion Processes* **1996**, *153*, 37−48.

(23) Eliel, E. L.; Wilen, S. H.; Mander, L. N. *Stereochemistry of Organic Compounds*; John Wiley and Sons: New York; 1994; p 23.

(24) Mártinez, A. G.; Vilar, E. T.; Fraile, A. G.; Martinez-Ruiz, P. *J. Phys. Chem. A* **2002**, *106*, 4942−4950 and references therein.

(25) Fitch, W. L.; Sauter, A. D. *Anal. Chem.* **1983**, *55*, 832−835.

(26) Syrstad, E. A.; Tureček, F. *J. Phys. Chem. A*, **2001**, *105*, 11144−11155.

(27) McMillen, D. F.; Golden, D. M. *Annu. Rev. Phys. Chem.* **1982**, *33*, 493−532.

(28) Gilbert, R. G.; Smith, S. C. *Theory of Unimolecular and Recombination Reactions*; Blackwell: Oxford, 1990; p 54.

(29) (a) Wolken, J. K.; Tureček, F. *J. Phys. Chem. A*, **1999**, *103*, 6268−6281. (b) Wolken, J. K.; Tureček, F. *J. Am. Chem. Soc.* **1999**. *121*, 6010−6018. (c) Gerbaux, P.; Tureček, F. *J. Phys. Chem. A*, **2002**, *106*, 5938−5950.

(30) Uggerud, E. *Adv. Mass Spectrom.* **1995**, *13*, 53−70.

(31) Traeger, J. C. *Int. J. Mass Spectrom.* **2000**, *194*, 261−267.

(32) Traeger, J. C.; McLoughlin, R. G.; Nicholson, A. J. C. *J. Am. Chem. Soc.* **1982**, *104*, 5318−5322.